Mott-Hubbard metal-insulator transition in d=∞

N. Blümer(1), R. Bulla(1), J. Schlipf(1), M. Jarrell(2), P. G. J. van Dongen(1), S. Kehrein(3), Th. Pruschke(4), and D. Vollhardt(1),
(1)Universität Augsburg, Germany, (2)University of Cincinnati, USA, (3)Harvard University, USA, (4)Universität Regensburg, Germany

Introduction

- Mott-Hubbard metal-insulator transition: transition between paramagnetic metal and paramagnetic insulator due to electronic interactions. Example: V_2O_3 doped with Cr.
- Standard model to describe transition: half-filled single-band Hubbard model:

$$H = -t \sum_{\langle i,j \rangle, \sigma} c^\dagger_{i\sigma} c_{j\sigma} + U \sum_i n_{i\uparrow} n_{i\downarrow} \qquad (1)$$

- DMFT: mapping of Hubbard model onto SIAM + self-consistency equation (exact in the limit $d \to \infty$)[2]. Lattice enters only via non-interacting density of states (DOS); here: semi-circular DOS of Bethe lattice.
- Units: non-interacting bandwidth $W = 4$.
- Controversial question: crossover / second order transition / first order transition within DMFT? Can the Hubbard model (within DMFT) explain the first order transition of V_2O_3?

Quantum Monte Carlo simulations

Impurity problem, determined by the effective action

$$S_{\text{eff}} = -\int_0^\beta d\tau\, d\tau' \sum_\sigma c^\dagger_\sigma(\tau) \mathcal{G}_0^{-1}(\tau-\tau') c_\sigma(\tau') + U \int_0^\beta d\tau \left(c^\dagger_\uparrow(\tau) c_\uparrow(\tau) - \frac{1}{2}\right)\left(c^\dagger_\downarrow(\tau) c_\downarrow(\tau) - \frac{1}{2}\right).$$

is solved by

- discretization of imaginary time into $\Lambda \approx 50-250$ slices of width $\Delta\tau = \beta/\Lambda$, Trotter decomposition
- Hubbard-Stratonovich transformation: introduces auxiliary Ising spins, allows for application of Wick's theorem
- instead of summing over all 2^Λ Ising configurations, about $\Lambda \cdot 300000$ are picked by Monte-Carlo importance sampling
- self-consistent iteration scheme (including Dyson's equation):

choose initial self energy Σ

$G^\sigma_{\alpha n} = \int d\epsilon \rho(\epsilon)/(i\omega_n + \mu - \Sigma(i\omega_n) - \epsilon)$

$\mathcal{G}^\sigma_{\alpha n} = (\Sigma^\sigma_{\alpha n} - G^{\sigma\ -1}_{\alpha n})^{-1}$

$G^\sigma_{\alpha n} = - < \Psi^\sigma_{\alpha n} \Psi^{\sigma\ *}_{\alpha n} > \Longleftarrow \mathcal{G}^\sigma_{\alpha n}$ (QMC, parallel)

$\Sigma_{new\,\alpha n} = \mathcal{G}^{\sigma\ -1}_{\alpha n} - (G^\sigma_{\alpha n})^{-1}$

iterate $\Sigma = \Sigma_{\text{new}}$ until $||\Sigma - \Sigma_{\text{new}}|| < \eta_{\max}$

- each iteration requires discrete Fourier transformation (plus inverse)

Double occupancy, compressibility, and effective mass

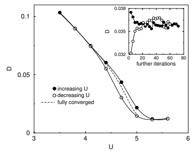

Fig. 1: QMC: double occupancy D at $T = 1/20$ using criterion $\eta_{\max} \leq 10^{-3}$. Inset: Vanishing of hysteresis with further iterations at $T = 0.05$, $U = 5$, $\Delta\tau = 0.3$

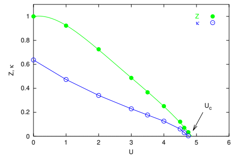

Fig. 2: QMC: compressibility κ and quasi-particle renormalization factor $Z = m/m^*$ vs. U for $T = 1/15$. Mott-Hubbard transition occurs at $U = U_c$ where $Z(U), \kappa(U) \to 0$

Single-particle spectra

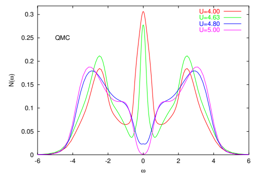

Fig. 3a: QMC/MEM results for the DOS for various values of U at $T = 1/20$, and $\Delta\tau = 0.17$. The gap opens at $U \simeq 5.0$.

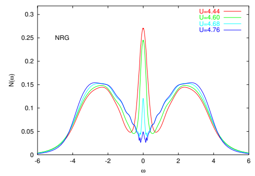

Fig. 3b: NRG results for the DOS for various values of U at $T = 1/20$. The transition occurs at $U \simeq 4.8$. No hysteresis is observed.

Phase diagram of the Hubbard model within DMFT

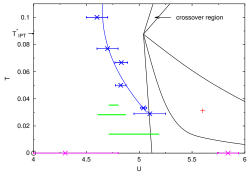

Fig. 4a: Status by 1999: Coexistence region from ED (-) and IPT (-)[1]; coexistence point within QMC (+)[2]; transition line from QMC (X)[3]. For $T = 0$: $U_{c1/2}$ from ED/PSCT/NRG (X) [1,4,5] and RDA (O) [6].

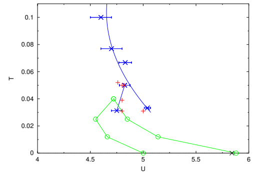

Fig. 4b: Phase diagram 2000. X: metal-insulator transition calculated with QMC. O: coexistence region within NRG. +: coexistence points from QMC by Rozenberg [7].

NRG solution of the DMFT equations

1. Logarithmic discretization

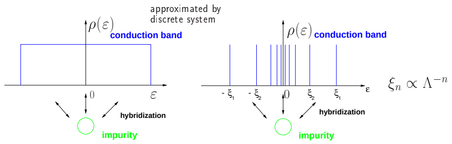

2. mapping on semi-infinite chain

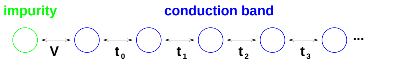

with exponentially decreasing hopping matrix elements $t_n \propto \Lambda^{-n/2}$

3. iterative numerical diagonalization

→ eigen-energies, matrix elements ⟶ static and dynamic properties

Conclusions

discussion of NRG results:

- for $T < T^*$: two solutions (metallic/insulating) within $U_{c,1} < U < U_{c,2}$;
- NRG applicable for arbitrarily low temperatures / large U; results depend on discretization Λ ($\Lambda \to 1$ exact).
- phase boundaries in good agreement with PSCM for $U_{c,2}$ at $T = 0$ and QMC for $T \approx T^*$; spectra for $T = 0.5$ in agreement with QMC-MEM;

discussion of QMC results:

- no hystereses for $T > T^* \approx 0.05$
- two solutions of self-consistency equations at $T = 1/32$
- metallic solution is more stable in coexistence region.

Results from fundamentally different methods now converge towards a reliable phase diagram.

References

[1] A. Georges *et al.*, Rev. Mod. Phys. **68**, 13 (1996).
[2] M. J. Rozenberg, G. Kotliar, and X. Y. Zhang, Phys. Rev. B **49**, 10181, (1994).
[3] J. Schlipf *et al.*, Phys. Rev. Lett. **82**, 4890 (1999).
[4] G. Moeller et al., Phys. Rev. Lett. **74**, 2082 (1996)
[5] R. Bulla, Th. Pruschke, and A. C. Hewson, J. Phys. Condens. Matter **10**, 8365 (1998)
[6] R. Noack and F. Gebhard, Phys. Rev. Lett. **82**, 1915, (1999)
[7] M. J. Rozenberg, R. Chitra, and G. Kotliar, Phys. Rev. Lett. **83**, 3498 (1999).